Integral Design and Manufacturing Methodology of a Reduced-Scale Servo Press

Jon Olaizola, Ekaitz Esteban, Javier Trinidad, Aitzol Iturrospe, Lander Galdos, Jose Manuel Abete and Eneko Saenz de Argandoña.

***Abstract*—In a context where industrial production boosts both the society and the economy of a country, improvements in industrial processes are key factors for efficient and reliable development of goods and products. New industrial processes and machines must be evaluated before deployment at large production scales. This paper proposes a new optimized design and manufacturing methodology to develop scaled test benches under predefined design requirements and constraints. The main contribution of this paper is the integral scaling methodology based on an optimized dimensional analysis and a similitude metric that eases the design of a test bench. Thus, the search for the optimal physical magnitudes of the test bench is accelerated and the inability to design non-proportional components is solved avoiding distortion. The first step of the methodology is definition of scaling laws through the Buckingham's π theorem. The second step is to employ a constrained optimization to determine the physical magnitudes of the test bench, based on the scaling laws defined earlier. The third step is to calculate the parameter activities and to set the design tolerances of the scaled components, so that the components are designed more freely while dealing with non-proportional ratios obtained due to arbitrary constraints. The methodology was used to construct a test bench of a servo press that retains the kinematics and dynamics of an industrial servo press. Experimental assessment of the dynamic and kinematic similitudes showed a less than 5% deviation from the industrial servo press's force/angular position ratio.**

***Index Terms*—Test bench, Buckingham's π, Kinematic and dynamic scaling, Optimization, Activity analysis, Servo press, Electromechanics.**

I. Introduction

SCALED test benches that keep a dynamic and kinematic similitude with the original system allow the testing of multiple machine configurations and experiments as if they were tested in the original machine [1]. Scaled systems save time and money since the original machine does not need to be stopped to carry out a set of new experiments. The development of such scaled machines can be part of a more generalized integrated design framework where several iterations are carried out in order to obtain the final product or machine as stated by Zhang et al. [2]. New monitoring and control strategies can be also applied in a straightforward manner in scaled test benches before they are deployed in actual industrial machines. Using this strategy, Brennan and Alleyne designed and evaluated a scaled test bench of a vehicle and roadway for safe and economic testing of a vehicle control application [3]. The scaled vehicle and the roadway kept dynamic and kinematic similitude with the original vehicle and roadway, thereby providing a means to attempt several control strategies before adopting one for full-sized vehicles. Recently, Esteban et al. presented a scaled elevator system for testing different electrical and mechanical configurations in controlled lab conditions [4]. The purpose of that study was to develop an elevator test bench that could emulate the original elevator's dynamics to allow testing of condition-monitoring algorithms.

According to Coutinho et al. [5], authors have mainly used two methods during the last decades to design and manufacture mechanical systems based on similitude theory: the differential equations method and dimensional analysis. The similitude theory states the necessary and minimum conditions of similarity that a new system or machine must retain with the original system so that its dynamics and kinematics are representative of the original system. Both methods take advantage of the system's magnitudes, as expressed in a model equation that explains the dynamic behavior of the system. Unlike the differential equation method, which simulates the dynamic model to carry out the scaling of a test bench, dimensional analysis does not employ the model equation but only the model magnitudes.

A dynamic model equation is described by state variables, inputs and parameters [6], [7]. State variables and inputs are variable magnitudes that represent the state of the system and the perturbations to which the system is subjected respectively. The parameters are invariant (or slowly varying) magnitudes that describe the characteristic or condition of the system components, such as mass, inertia and elastic constant.

Dimensional analysis is the simplest scaling method. Unlike the differential equations method, where dynamic and kinematic similitude are assessed by trial-and-error, dimensional analysis evaluates similitude by non-dimensional relationships among system magnitudes [5]. Dimensional analysis elaborates scaling laws based on the Buckingham's π method proposed by Vaschy [8].

The Buckingham's π theorem gathers a system's physical magnitudes in the so-called π-groups/terms, which derive in scaling laws. A physical magnitude is a property of a physical process or system that can be measured and defined with a

Manuscript received January 21, 2020.

J. Olaizola is with the Department of Electronic and Computer Science, Mondragon Unibertsitatea, Arrasate, 20500 Spain (e-mail: jolaizolaa@mondragon.edu)

J. Trinidad, E. Sàenz de Argandoña, Jose Manuel Abete and Lander Galdos are with the Department of Mechanics and Industrial Production, Mondragon Unibertsitatea, Arrasate, 2500 Spain (e-mail: jtrinidad@mondragon.edu; esaenzdeargan@mondragon.edu; jmabete@mondragon.edu; lgaldos@mondragon.edu).

E. Esteban and A. Iturrospe are with Promotion and Development of Automatic Systems (PDSA), Arrasate, 2500 Spain (e-mail: aiturrospe@mondragon.edu; eesteban@mondragon.edu).

number and a unit. Length, mass, voltage etc. are examples of physical magnitudes. The π-groups are formulated so their product yields a dimensionless result. To guarantee a perfect dynamic and kinematic similitude between the scaled system and the original, the π-groups must yield the same numerical result.

Dimension analysis has been widely applied to scale test benches in several engineering areas. For example, Simitses and Rezaeepazhand applied dimensional analysis to design scaled laminated beam-plates [9]. They assumed that the physical properties of both the original and the scaled beam-plate were the same, which eases the definition of the rest of the physical magnitudes based on the formulated π-groups. Nonetheless, they also pointed out that changing the scale factors of some magnitudes would derive a complete new set of magnitude values, which would have to be recalculated. Similarly, Verma et al. developed a scaled vehicle whose longitudinal and power-train dynamics kept a dynamic similitude with a full-size, high-mobility multipurpose wheeled vehicle [10]. The authors guaranteed the dynamic similitude of both vehicles by modifying both vehicles (the test bench and the full-scale one) and introducing distorted scaling laws [11] to compensate for unfeasible combinations of magnitudes.

Distortion is a widely used mechanism when unfeasible characteristics of components or material are obtained from the scaling laws. Distortion is simply a corrective factor that has to be multiplied to the scaling laws to ensure that dynamic similitude is met. Recently, Esteban et al. presented a design methodology of a scaled elevator system for fault detection and diagnosis [4]. Due to the infinite optimal combinations of the scaled physical magnitudes that could be established by means of the defined scaling laws, those authors settled a design specification sheet and conducted a least squares-based optimization. Nevertheless, the authors had to perform numerous optimization runs before providing a scaled elevator with suitable size/capabilities specifications. The authors also had to distort the scaling laws concerning the power-train and the guiding system of the scaled test bench due to the unfeasible geometric proportions they obtained from their scaling procedure.

Luo et al. also employed the Buckingham's π-based dimensional analysis to design and manufacture a test bench with different models of blade-integrated disks (blisks) [12]. Those authors also had to use distorted scaling laws to replicate the dynamics of the different models of blisks that are extensively used in different applications, such as gas turbines, steam turbines or aero engines. The reader can find more examples of dimensional analysis scaling with distorted scaling laws in [13]–[15].

Zhou and Li proposed to overcome the similitude distortion introduced by distorted scaling laws by use of the so-called equivalent similar method to scale the dynamic characteristics of stiffened cylindrical shells [16]. Before defining the scaling laws, the authors carried out a process of equivalence by interrelating the different magnitudes that participate in the model equations based on their dependence on each other. Thus, they were able to design the components of their use case more freely. Although their methodology successfully improves the limitation of distorted test bench designs, the method has two handicaps. One is that the equivalent method includes an integration of the system parameters that makes simplifying assumptions in order to reduce the amount of parameters involved in the model equation. The removal of parameters from dynamic model equations in motional systems is unfeasible as they contribute to the kinematics of the system. The second limitation is that all the independent parameters are mainly fixed to preset values; therefore, they cannot evaluate whether the scaling of the system is optimal.

The present paper proposes a design and manufacturing methodology for developing a scaled test bench that is able to reproduce the dynamics and kinematics of the original system, based on the dimensional analysis. The methodology overcomes the limitations found in the literature by applying static optimization and tolerance-based design approaches. The physical magnitudes included in the dynamic model equation of the system are optimally defined through the optimization approach conducted based on the constraints and design variables formulated from requirements. The constrained optimization solves the multiple iterations involved in the definition of the system magnitudes. The similitude distortion derived from practical design limitations is also addressed by carrying out an activity-based analysis [1] to identify parameters with negligible contribution to the system dynamics. Hence, no distortion of scaling laws is required and some components of the test bench can be designed more freely. The proposed integrated design and manufacturing methodology is significantly different from the concurrent integrated design methodologies by use of optimization techniques, e.g. [17] in that they cannot solve the scaled design problem.

The rest of the paper is organized as follows. Section II presents the proposed design and manufacturing methodology for the kinematic and dynamic scaling of test benches. Section III describes the dynamic model equation of an industrial servo press and shows the application of the methodology to design and manufacture a scaled version of an industrial servo press. Section IV shows the experimental results of the manufactured test bench and compares the dynamics and kinematics of the test bench and the original servo press. Finally, section V gathers some conclusions and suggests future lines of research.

II. Methodology

Similitude-based scaling arises from the basic theorem of dimensional analysis, also known as Buckingham's π theorem [18], [19]. This theorem provides a methodology for formulating dimensionless scaling laws from a system's magnitudes. The obtained scaling laws must yield the same results using the physical magnitudes of the original system and the scaled magnitudes of the test bench to keep the dynamic similitude between both systems. Buckingham's π theorem does not concern the proportions of the physical magnitudes of components, but it guarantees that the dynamic behavior of the scaled machine will be similar to that of the original system.

Formulated scaling laws offer the possibility of scaling the test bench in multiple ways. In this study, the size and characteristics of the scaled test bench are limited by assessing

those scaling laws in a static optimization framework to obtain optimal values of magnitudes according to the predefined requirements and constraints.

When designing the components of the test bench, as established by the optimal physical magnitudes, the designer may encounter difficulties due to unfeasible characteristics of the components. This limitation is overcome by proposing design tolerances based on the importance of the parameters in the performance of the test bench's dynamic behavior. The importance of the parameters is measured in the activity analysis.

A. Buckingham's π formulation

Let us assume a dimensional expression (1) that includes U physical magnitudes s of the analyzed dynamic system.

$$z = g(s_u) \qquad u = 1, 2, .., U \tag{1}$$

Physical magnitudes are formed by fundamental dimensions denoted as M = mass, L = length and T = time. Some physical magnitudes such as the mass $m(kg) = M$, have one fundamental dimension, while others such as the linear acceleration $a(m/s^2) = LT^{-2}$, have more than one. Let us define Q as the number of fundamental dimensions among all the physical magnitudes s_u. Buckingham's π theorem then determines that the U magnitudes can be arranged in $(U-Q)$ dimensionless equations known as π-groups.

The π-groups are constructed using as many repeating magnitudes j as Q, each one including at least one of the fundamental dimensions. The most frequently chosen repeating magnitudes are those that are a-priori known or easily measurable. Thus, a π-group is represented as in (2).

$$\begin{gathered} \pi_n = s_n (j_1)^{\alpha_1} (j_2)^{\alpha_2} ... (j_q)^{\alpha_q} \\ n = 1, 2, ..(U-Q) \quad q = 1, 2, ..Q \end{gathered} \tag{2}$$

where $\alpha_1, \alpha_2, \alpha_q$ are chosen to ensure each π_n-group is non-dimensional. These π-groups can be used to define scaling laws λ for each scaled magnitude of the system as expressed in (3).

$$\lambda_n = \frac{\pi_{n_t}}{\pi_{n_o}} \qquad \lambda_{s_u} = \frac{s_{u_t}}{s_{u_o}} \tag{3}$$

where sub-indexes t and o stand for the test bench and the original system respectively.

B. Optimization of the scaled system's physical magnitudes

Unlike for an ideal scaling framework, where the system's magnitudes can be scaled faithfully according to the established requirements, sometimes the design of the scaled system is subjected to constraints, such as geometric constraints that have to do with the kinematics of scaled system, dynamic constraints related to the dynamic behavior or operational constraints that limit the maximum and minimum operation ranges of the mechatronic system. In this context, achieving the required scaling of the system may be tedious. To overcome this difficulty a static convex optimization approach is proposed, which provides optimal values for the test bench's magnitudes keeping the dynamic and kinematic similitude with the original system. The optimization must also satisfy some operational and geometric requirements and constraints.

The optimization approach is stated as a minimization of a cost function $f(\lambda_{s_u})$ defined from the design requirements and subject to constraints. A design requirement can be any operational specification that the scaled test bench must guarantee, keeping at the same time the dynamic and kinematic similitude with the original system, e.g. a proportional torque to rotate a scaled servomotor at the same constant speed as the original servomotor. The constraints are usually given by geometric specifications and operational limits $h(\lambda_{s_u})$ of the scaled system, such as length, width, mass, maximum and minimum speed, voltage, force, pressure and so on.

Some of the scaling laws obtained from the Buckingham's π formulation are used as design variables, whilst others are used as constraints of the scaled system. Maximum and minimum values of the test bench's magnitude ratios are also used as boundaries to delimit the capabilities of the test bench. The optimization problem is expressed as in (4).

$$\begin{aligned} &\min_{\boldsymbol{\lambda_s}} f(\boldsymbol{\lambda_s}) \qquad \boldsymbol{\lambda_s} \in \Lambda_s \\ \text{s.t.} \quad &h_i(\boldsymbol{\lambda_s}) = 0 \qquad i = 1, ..., I \\ &\lambda_{s_{u_{min}}} \leqslant \lambda_{s_u} \leqslant \lambda_{s_{u_{max}}} \end{aligned} \tag{4}$$

where $\lambda_{s_{u_{min}}}$ and $\lambda_{s_{u_{max}}}$ represent the minimum and maximum values the physical magnitude ratios can take in the optimization approach, based on the maximum and minimum values of their corresponding physical magnitudes.

The optimization algorithm is executed until Karush-Kuhn-Tucker (KKT) optimality conditions [20] are satisfied in a local or global minimum. The optimized values of the system's magnitudes describe a scaled system that keeps the dynamic and kinematic similitude with the original system.

C. Definition of design tolerances

Some physical magnitudes included in the scaling methodology, such as masses, inertia and geometric characteristics of components, are known as system static parameters, since they do not change during the working cycle of the system. On occasion, the constrained optimization of the physical magnitudes can yield values that are difficult or even impossible to obtain when designing a component. Deviations introduced in the design of the components and in their manufacturing may affect, to some degree, the dynamics and kinematics of the test bench. Quantifying the effect these inevitable deviations will cause in the dynamics of the systems is therefore important, as is determining the impact of each parameter on the dynamics of the system. This determination will allow relaxation of the specifications of components parameters with less activity, easing the design of the test bench components.

Some parameters have a greater impact than others on the dynamic behavior; therefore, their tolerance with respect to the optimized values should be lower to keep the kinematic and dynamic similitude. On the contrary, deviations in parameters that have less impact on the dynamic behavior produce a

minor change in the dynamics of the system. The influence of a system's parameters is determined by analyzing each parameter's activity, which is a measurement of the amount of energy a parameter of the system consumes and generates over a specified time window T. The activity sheds light on the sensitivity of a parameter on the dynamic behavior of the system. Activity is defined as in (5).

$$A_x = \int_{t=0}^{T} |P_x(t)|dt \qquad x = 1, 2, ..., X \tag{5}$$

Here $|P_x(t)|$ is the absolute value of the parameter's power over the time window T and X is the number of parameters p of the system.

According to the activity analysis, the parameters with the smallest activities tolerate a larger deviation from the optimized values without significantly altering the dynamic behavior of the test bench to be manufactured. The tolerance of the parameters' values is specified by the grade of similitude required by the designer and is calculated based on the sensitivity Ω of the analyzed parameter as in (6). The sensitivity measures the percentage by which the activity of a parameter changes due to its deviation (Δs_x) with respect to a benchmark. The benchmark is the activity of a parameter calculated for the value obtained in the optimization.

$$\Omega_x = \frac{A_x(\Delta s_x)}{\sum_{x=1}^{X} A_x} \times 100 \tag{6}$$

This methodology leads to a more flexible design and manufacturing procedure for scaled test benches. The definition of tolerances based on the activity and sensitivity analysis also allows a reduction in manufacturing costs while keeping a high degree of dynamic and kinematic similitude with the original system. Fig. 1 describes the three stages of the methodology, along with the tasks carried out within each of the stages.

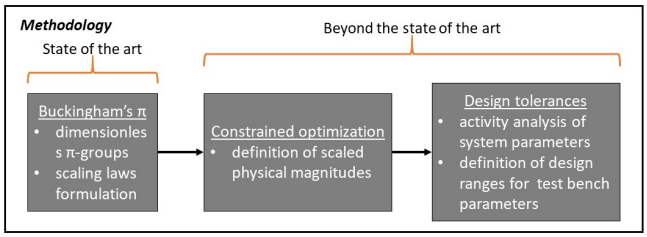

Fig. 1. Stages and of the proposed design and manufacturing methodology.

III. Application of the Methodology for the Design and Manufacturing of a Reduced Scale Servo Press Test Bench

The proposed methodology has been used to construct a reduced scale test bench of an industrial servo press, providing it the ability of emulating the dynamic and kinematic behaviors of the original system. The purpose of manufacturing the test bench is to provide a means of testing different machine conditions and experiments as if they were conducted in the original servo press. The test bench will also be useful for predicting the behavior of the industrial servo press before the new manufacturing processes are implemented in the industrial production line.

A. Model of the servo press

As presented in [21], a servo press is a mechatronic system composed of an electric servomotor and a mechanical kinematic chain that transforms the torque transmitted by the servomotor into process force. This process force is the magnitude that shapes the produced part by means of a die.

The mechanical kinematic chain of the analyzed servo press is formed by a gearbox, a crankshaft, two connecting rods and a ram, as illustrated in Fig 2. The ram slides through a guiding system that maintains the parallelism of the ram with respect to the bed of the servo press. The bed of the press is installed on the bolster, which also supports the frame of the servo press. A load balancer counteracts the weight of the ram, so the servomotor does not have to produce an excessive torque to move the ram. The load balancer is a pressured chamber whose force depends directly on the inner pressure of the air and the area of the chamber.

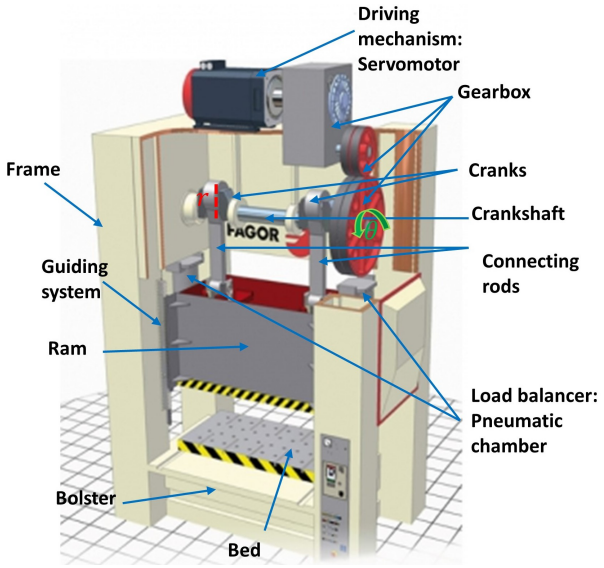

Fig. 2. Common components of metal forming press (Courtesy of Fagor Arrasate).

The dynamic model equation of the servo press is shown in (7), whose physical magnitudes are listed in Table I. Three magnitudes of Table I are excluded from the scaling methodology for different reasons. The scaling of the gearbox is excluded from the dimensional analysis. Since the gearbox (as well as the servomotor) is a commercial device, it will be selected based on the torque and the speed obtained from the optimization step. Therefore, the value of η will be implicit in τ_e for the dynamic analysis, which actuates directly over the crankshaft. Likewise, the friction torque cannot be scaled, since it will depend on factors that cannot be scaled, such as lubrication, the finishing of the manufactured components or the assembly of the system. The load balancer has not been taken into account either, since its selection wholly depends on the mass of the ram, and it will therefore be selected once the ram is designed.

$$M(\theta)\ddot{\theta} + N(\theta)\dot{\theta}^2 + G(\theta) = \tau_e\eta - \tau_{fric} - (F_{ms} + F_{lb})\, r\sin\theta\left(1 + \frac{r\cos\theta}{c}\right) \quad (7)$$

where $M(\theta)$, $N(\theta)$ and $G(\theta)$ are defined in (8), (9) and (10) respectively,

$$M(\theta) = \left(I_1 + m_1\acute{r}^2 + \frac{I_2 r^2\cos^2\theta}{c^2} + \frac{\left(l-\acute{l}\right)^2}{l^2} m_2 r^2\cos^2\theta + \sin^2\theta\left(m_2 r^2 \frac{\left(r\acute{l}\cos\theta + lc\right)^2}{l^2c^2} + m_3 r^2 \frac{(r\cos\theta + c)^2}{c^2}\right) + I_4 + I_5\eta_4^2 + I_6\left(\eta_4\eta_5\right)^2 + I_7\left(\eta_4\eta_5\eta_6\right)^2\right) \quad (8)$$

$$N(\theta) = \frac{1}{2}\left(\frac{2I_2 r^4\cos^3\theta\sin\theta}{c^4} - \frac{2I_2 r^2\cos\theta\sin\theta}{c^2} - \frac{2m_2 r^2\cos\theta\sin\theta\left(l-\acute{l}\right)^2}{l^2} + 2\sin\theta\cos\theta \left(m_2 r^2\frac{\left(r\acute{l}\cos\theta + lc\right)^2}{l^2c^2} + m_3 r^2\frac{(r\cos\theta + c)^2}{c^2}\right) + 2\sin^2\theta\left(\frac{m_2 r^3\acute{l}\sin\theta\left(r\acute{l}\cos\theta + lc\right)(r\cos\theta - c)}{l^2c^4} \frac{(r\cos\theta + c)}{l^2c^4} + \frac{m_3 r^3\sin\theta(r\cos\theta + c)^2(r\cos\theta - c)}{c^4}\right)\right) \quad (9)$$

$$G(\theta) = g\left(\sin\theta\left(m_1\acute{r} + m_2 r + m_3 r\right) + \sin\theta\cos\theta \left(\frac{m_2 r^2\acute{l}}{lc} + \frac{m_3 r^2}{c}\right)\right) \quad (10)$$

and $c = \sqrt{l^2 - r^2\sin^2\theta}$.

TABLE I
SYMBOLS OF SERVO PRESS MODEL

States	
θ, $\dot{\theta}$, $\ddot{\theta}(rad, \frac{rad}{s}, \frac{rad}{s^2})$	Angular position, speed and acceleration of the crankshaft
Parameters	
$g = 9.81\frac{m}{s^2}$	Gravitational acceleration constant
$I_1 = 80.72kgm^2$	Inertia of the crankshaft
$m_1 = 424kg$	Mass of the crankshaft
$I_2 = 132.72kgm^2$	Inertia of the connecting rods
$m_2 = 424kg$	Mass of the connecting rods
$m_3 = 11600kg$	Mass of the ram
$r = 0.2m$	Radius of the crank
$\acute{r} = 0.0762m$	Distance between the axis of the crank and its center mass
$l = 1.05m$	Length of the connecting rod
$\acute{l} = 0.327m$	Distance between the connecting rod's axis and its center mass
$I_4 = 105.77kgm^2$	Inertia of the 1st gear of the gearbox
$I_5 = 19.007kgm^2$	Inertia of the 2nd gear of the gearbox
$I_6 = 3.58kgm^2$	Inertia of the 3rd gear of the gearbox
$I_7 = 7.38kgm^2$	Inertia of the servomotor's rotor
$\eta_4 = 60/17$	Reduction ratio of the 1st gear of the gearbox
$\eta_5 = 60/17$	Reduction ratio of the 2nd gear of the gearbox
$\eta_6 = 71/18$	Reduction ratio of the 3rd gear of the gearbox
$\eta = \eta_4\eta_5\eta_6$	Reduction ratio of the gearbox
Inputs	
$F_{ms}(N)$	Force of the process
$F_{lb}(N)$	Force of the load balancer
$\tau_e(Nm)$	Electric torque of the servomotor
$\tau_{fric}(Nm)$	Friction torque

B. Application of the methodology

The magnitudes to be scaled are included in the dimensional expression, as shown in (11).

$$z = g(\tau_e, \theta, \dot{\theta}, \ddot{\theta}, r, \acute{r}, l, \acute{l}, I_1, m_1, I_2, m_2, m_3, F_{ms}, \xi, x) \quad (11)$$

where the symbols that have not been already defined in the previous subsection are ξ and x, representing the elastic coefficient and the linear deformation of the servo press's structure, respectively. These two magnitudes are implicitly included in the process force, since they define the force that the servo press structure exerts against the formed workpiece ($F_{ms} = \xi x$). F_{ms} denotes the maximum process force value of the servo press, which will be the main design requirement. Equation (11) shows $U = 16$ scalable magnitudes, whose fundamental dimensions are listed in Table II.

TABLE II
FUNDAMENTAL DIMENSIONS OF SERVO PRESS MAGNITUDES

Magnitude	Dimension	Magnitude	Dimension
τ_e	ML^2T^{-2}	(I_1, I_2)	ML^2
θ	none	(m_1, m_2, m_3)	M
$\dot{\theta}$	T^{-1}	F_{ms}	MLT^{-2}
$\ddot{\theta}$	T^{-2}	ξ	MT^{-2}
$(r, \acute{r}, l, \acute{l})$	L	x	L

The dimensional analysis of the magnitudes gathered in Table II show $Q = 3$ fundamental dimensions (M,L and T). Thus, $(U - Q) = 13$ non-dimensional π-groups can be formulated by means of Q repeating magnitudes selected by convenience. The selected repeating magnitudes are $j_1 = F_{ms}$, $j_2 = m_3$ and $j_3 = r$, since they can be easily measured in the original servo press. The π-groups are shown in Table III. The π_1-group calculation procedure is demonstrated in Appendix A.

TABLE III
π-GROUPS FORMED BY SERVO PRESS'S MAGNITUDES

$\boldsymbol{\pi_1}$	$\frac{\tau_e}{F_{ms}r}$	$\boldsymbol{(\pi_8, \pi_9)}$	$\frac{(I_1,I_2)}{m_3 r^2}$
$\boldsymbol{\pi_2}$	θ	$\boldsymbol{(\pi_{10}, \pi_{11})}$	$\frac{(m_1,m_2)}{m_3}$
$\boldsymbol{\pi_3}$	$\dot{\theta}\sqrt{\frac{m_3 r}{F_{ms}}}$	$\boldsymbol{\pi_{12}}$	$\xi\frac{r}{F}$
$\boldsymbol{\pi_4}$	$\dot{\theta}\frac{m_3 r}{F_{ms}}$	$\boldsymbol{\pi_{13}}$	$\frac{x}{r}$
$\boldsymbol{(\pi_5, \pi_6, \pi_7)}$	$\frac{(\acute{r},l,\acute{l})}{r}$		

The π-groups lead to the formulation of the scaling laws λ_n, which describe the ratio between the physical magnitudes of the original system and the scaled test bench. The scaling law constructed from π_1 is shown in (12). Scaling laws are grouped as in the Table IV.

$$\pi_1 \rightarrow \frac{\tau_{e_o}}{F_{ms_o} r_o} = \frac{\tau_{e_t}}{F_{ms_t} r_t} \rightarrow \frac{F_{ms_t} r_t}{F_{ms_o} r_o} = \frac{\tau_{e_t}}{\tau_{e_o}} \rightarrow \lambda_{F_{ms}} \lambda_r = \lambda_{\tau_e} \tag{12}$$

TABLE IV
π-GROUPS FORMED BY SERVO PRESS'S MAGNITUDES

$\boldsymbol{\pi_1}$	$\lambda_{F_{ms}}\lambda_r = \lambda_{\tau_e}$	$\boldsymbol{(\pi_8, \pi_9)}$	$\lambda_{(I_1,I_2)} = \lambda_{m_3}\lambda_r^2$
$\boldsymbol{\pi_2}$	$\lambda_\theta = 1$	$\boldsymbol{(\pi_{10}, \pi_{11})}$	$\lambda_{(m_1,m_2)} = \lambda_{m_3}$
$\boldsymbol{\pi_3}$	$\lambda_{\dot{\theta}} = \frac{\lambda_{F_{ms}}^{1/2}}{\lambda_{m_3}^{1/2}\lambda_r^{1/2}}$	$\boldsymbol{\pi_{12}}$	$\lambda_\xi = \frac{\lambda_{F_{ms}}}{\lambda_r}$
$\boldsymbol{\pi_4}$	$\lambda_{\ddot{\theta}} = \frac{\lambda_{F_{ms}}}{\lambda_{m_3}\lambda_r}$	$\boldsymbol{\pi_{13}}$	$\lambda_x = \lambda_r$
$\boldsymbol{(\pi_5, \pi_6, \pi_7)}$	$\lambda_{(\acute{r},l,\acute{l})} = \lambda_r$		

The obtained scaling laws are used in a static sequential quadratic programming (SQP) algorithm executed in MATLAB using the *fmincon* function. The *fmincon* function includes constraints and a single design variable-based cost function. The cost function is defined by the squared error between the objective maximum force ratio ($\lambda_{F_{ms}}$) and the optimal maximum force ratio ($\bar{\lambda}_{F_{ms_i}}$) provided by the optimization algorithm at each i iteration. Therefore, the cost function has no units. The optimization problem and the cost function are expressed in (13) and (14) respectively.

$$\min_{\lambda_{F_{ms}}} f\left(\lambda_{F_{ms}}\right) \tag{13}$$

$$f\left(\lambda_{F_{ms}}\right) = \left(\lambda_{F_{ms}} - \bar{\lambda}_{F_{ms_i}}\right)^2 \qquad \bar{\lambda}_{F_{ms_i}} = \bar{\lambda}_{\xi_i}\bar{\lambda}_{r_i} \tag{14}$$

At each i iteration, the optimization algorithm proposes values for $\bar{\lambda}_{\xi_i}$ and $\bar{\lambda}_{r_i}$ to obtain the optimal maximum force ratio $\bar{\lambda}_{F_{ms_i}}$ until the KKT optimality conditions are met for the cost function, either in a local or global optimum. The rest of the scaling laws are introduced in the algorithm as non-linear equality constraints $h_n(c_{eq_n})$, as in (15). There is the possibility that this problem is not convex because the equality constraint condition is not affine function. Then, the optimal solution depends on the initial conditions. Thus, the scaled physical magnitudes of the test bench must yield the same π-group values as the original system's magnitudes do, which guarantees retention of the kinematics and dynamics.

The design variables and constraints are provided to the optimization algorithm as inputs. In this case, the targeted design objective is that the test bench must carry out at least a process force up to $F_{ms} = 1000kgf$, which corresponds to a 1:400 scaled maximum force compared to the original servo press. The maximum size of the test bench is also defined as a boundary constraint by means of the displacement of the ram. The displacement of the ram d, which is given by $d = 2r$ is bounded by $[0.03, 0.04]m$.

$$\begin{aligned} c_{eq_1} &= \left(\frac{\lambda_{\tau_e}}{\lambda_{F_{ms}}\lambda_r} - 1\right) & c_{eq_2} &= \left(\frac{\lambda_{\dot{\theta}}\lambda_{m_3}^{1/2}\lambda_r^{1/2}}{\lambda_{F_{ms}}^{1/2}} - 1\right) \\ c_{eq_3} &= \left(\frac{\lambda_{\ddot{\theta}}\lambda_{m_3}\lambda_r}{\lambda_{F_{ms}}} - 1\right) & c_{eq_{(4,5,6)}} &= \left(\frac{\lambda_{(\acute{r},l,\acute{l})}}{\lambda_r} - 1\right) \\ c_{eq_{(7,8)}} &= \left(\frac{\lambda_{(I_1,I_2)}}{\lambda_{m_3}\lambda_r^2} - 1\right) & c_{eq_{(9,10)}} &= \left(\frac{\lambda_{(m_1,m_2)}}{\lambda_{m_3}} - 1\right) \\ c_{eq_{11}} &= \left(\frac{\lambda_\xi\lambda_r}{\lambda_{F_{ms}}} - 1\right) & c_{eq_{12}} &= \left(\frac{\lambda_x}{\lambda_r} - 1\right) \end{aligned} \tag{15}$$

All the scaling laws are initialized to 1 so that the SQP begins the search from the original servo press magnitudes. The SQP takes 14 iterations (with a priori undefined number of runs at each iteration) to obtain the optimal values of the scaling laws with the given initial conditions, yielding the minimum value of the cost function of $5.625{\times}10^{-5}$. The optimized values shown in Table V, are those that guarantee the dynamic and kinematic similitude. In regards to the optimized $\dot{\theta}$ and $\ddot{\theta}$, note that they represented the factors with which the speed and acceleration of the crankshaft must be increased in the test bench to keep the dynamic similitude with the industrial machine during the whole working cycle. These two factors compensate the non-proportional scaling of the magnitudes of components such as the mass and the inertia of connecting rods and the crankshaft, and they mainly contribute to the torque consumed during the whole working cycle of the press in moving the kinematic chain, so that λ_{τ_e} is kept constant.

TABLE V
ORIGINAL AND OPTIMIZED PHYSICAL MAGNITUDES' VALUES

Mag	Or Val	Opt val	$\boldsymbol{\lambda_{s_u}}$
τ_e	$9.081 \times 10^4 Nm$	$22.70Nm$	2.5×10^{-4}
θ	$(-)rad$	$(-)rad$	1
$\dot{\theta}$	$(X)rad/s$	$2.19(X)rad/s$	2.19
$\ddot{\theta}$	$(X)rad/s^2$	$4.82(X)rad/s^2$	4.82
r	$0.2m$	$0.02m$	0.1
$\acute{r}$	$0.076m$	$0.00762m$	0.1
l	$1.05m$	$0.105m$	0.1
$\acute{l}$	$0.3270m$	$0.0327m$	0.1
I_1	$80.92kgm^2$	$0.0045kgm^2$	5.5×10^{-5}
m_1	$424kg$	$2.35kg$	5.5×10^{-3}
I_2	$132.72kgm^2$	$0.0073kgm^2$	5.5×10^{-5}
m_2	$825.86kg$	$4.57kg$	5.5×10^{-3}
m_3	$11600kg$	$64.21kg$	5.5×10^{-3}
F_{ms}	$400000kgf$	$1000kgf$	2.5×10^{-3}
ξ	$1.35 \times 10^9 N/m$	$3.375 \times 10^7 N/m$	2.5×10^{-2}
x	$0.0025m$	$0.00025m$	0.1

The values obtained solving the π-groups for both the original system and the test bench, reveal an identical kinematic and dynamic similitude of the test bench according to the Buckingham's π theorem. Results are shown in Table VI. Therefore, π-groups reveal that the test bench's magnitudes are optimally scaled.

TABLE VI
π VALUES OF THE ORIGINAL AND OPTIMIZED PHYSICAL MAGNITUDES

π-groups	Original values	Optimized values
π_1	1.1351	1.1351
π_2	1	1
π_3	0.0762	0.0762
π_4	0.0058	0.0058
π_5	0.3811	0.3811
π_6	5.25	5.25
π_7	1.6351	1.6351
π_8	0.174	0.174
π_9	0.286	0.286
π_{10}	0.0366	0.0366
π_{11}	0.0712	0.0712
π_{12}	675	675
π_{13}	0.0125	0.0125

Difficulties may arise in designing the components specified by the optimized physical magnitudes; therefore, a procedure based on parameter activities and sensitivities is carried out in the third step of the methodology. Safety issues can make the designer consider a component too weak if designed under the specified optimal parameters, as in the case of the connecting rods. The designer of the test bench will define some ranges for the parameter values based on a tolerance defined by means of the sensitivity of parameters. A smaller tolerance defined for the test bench component parameters with respect to the optimal values, will result in a higher similitude with the dynamics and kinematics of the original servo press. At the same time, smaller tolerances can also imply higher manufacturing costs, since the required properties of the components, such as the weight and inertia, can be also more difficult to obtain.

The parameters of the test bench are m_1, m_2, m_3, I_1, I_2 and ξ, which define the condition of the test bench's components. Analytical expressions of the parameters' power are shown in Appendix B. Parameter activities are expressed in the set of equations (16).

$$\begin{aligned} A_{m_1} &= \int_{t=0}^{T} |P_{m_1}(t)|dt \qquad A_{m_2} = \int_{t=0}^{T} |P_{m_2}(t)|dt \\ A_{m_3} &= \int_{t=0}^{T} |P_{m_3}(t)|dt \qquad A_{I_1} = \int_{t=0}^{T} |P_{I_1}(t)|dt \\ A_{I_2} &= \int_{t=0}^{T} |P_{I_2}(t)|dt \qquad A_{\xi} = \int_{t=0}^{T} |P_{\xi}(t)|dt \end{aligned} \tag{16}$$

Optimized parameter activities are calculated numerically using the analytical expression of parameter power and the crankshaft's angular position θ as inputs for the calculation of power. The crankshaft's angular position is depicted in Fig. 3.

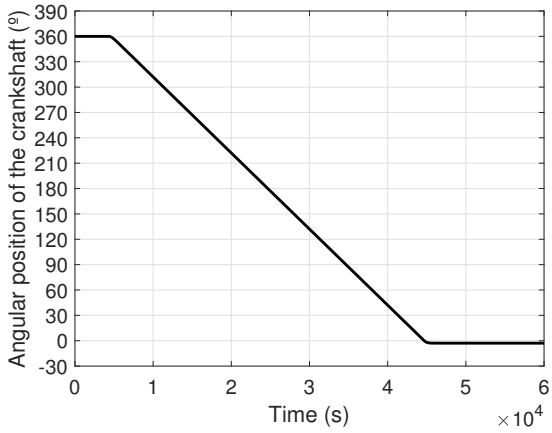

Fig. 3. The angular position of the crankshaft.

The activity values and their percentage of the total activity are shown in Table VII.

TABLE VII
PARAMETERS' ACTIVITIES

Parameters	Activity	Activity percentage
m_1	$0.7014J$	1.23%
m_2	$3.59J$	6.31%
m_3	$50.35J$	88.6%
I_1	$0.088J$	0.15%
I_2	$6.81 \times 10^{-4}J$	0.002%
ξ	$2.11J$	3.71%
Total	$56.84 \times 10^5 J$	100%

Fig. 4 shows the evolution of activities during the working cycle. The activity analysis reveals that a deviation in the ram's mass will have a greater impact on the kinematic and dynamic behavior of the system than will a deviation in other parameters, since the ram activity is 88.6% of the total activity. The activity of m_3 implies that the dynamic and kinematic behavior of the entire system are highly dependent on the mass of the ram.

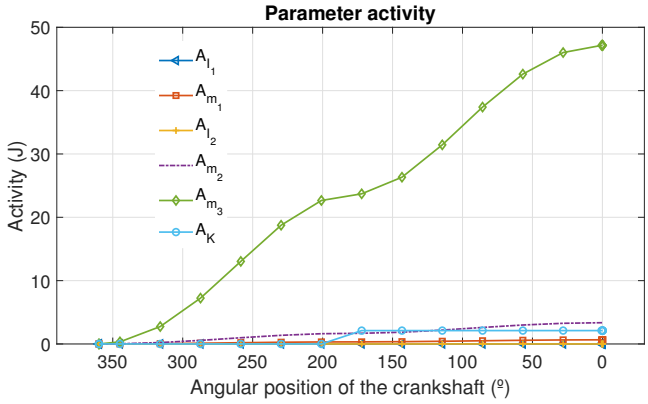

Fig. 4. Activities of parameters during a single cycle of the servo press.

Regarding the design and manufacturing of the scaled test bench, a tolerance of 2% in the parameter activities is set, which contributes to the definition of more relaxed design specifications of the components. Some components, such as the cranks and the connecting rods, would otherwise be much more expensive and difficult to manufacture due to the inertia, masses and lengths obtained in the optimization. The ranges of the parameters are shown in Table VIII. These ranges are calculated based on the sensitivity equation presented in (6), where Ω_x is replaced by the 2% tolerance, and the parameter values that generate that 2% of deviation are calculated. Table VIII also shows the actual values obtained after the design and manufacturing. For parameters with small activity percentages (less than 3%), values equal to or higher than the optimized values have been proposed, since components with smaller values were more difficult and expensive to manufacture due to the characteristics of the manufacturing material required. According to Table VIII, the obtained parameter values after the manufacturing process lie between the established minimum and maximum values.

TABLE VIII
PARAMETERS' MANUFACTURING RANGES

Par	Range	After manufacturing	
		Actual value	Activity %
m_1	$[2.35, 7.16]\,kg$	$6.058kg$	3.09%
m_2	$[3.24, 8.58]\,kg$	$7.24kg$	8.76%
m_3	$[42.23, 73.2]\,kg$	$60.12kg$	85.33%
I_1	$[0.0045, 0.1523]\,kgm^2$	$0.0101kgm^2$	0.154%
I_2	$[0.0073, 2.4]\,kgm^2$	$0.0410kgm^2$	0.006%
ξ	$[2.66{\times}10^7, 4.76{\times}10^7]\,N/m$	$3.06{\times}10^7 N/m$	2.66%

The entire test bench was manufactured by means of a machining process and is shown in Fig. 5. The servomotor that drives the operation of the press is OMRON's model R88M-1M1K020C-S2(Q), which is able to exert up to $4.77Nm$ in continuous operation, and it is controlled by means of OMRON's NJ301-1100 controller. The servomotor is attached to the crankshaft through APEX DYNAMICS's PEIIR090-I7 elbowed gearbox with a reduction ratio of $\eta = 7$. Thus, the assembly formed by the servomotor and the gearbox can exert up to $33.39Nm$ in the absence of inefficiencies in the kinematic chain.

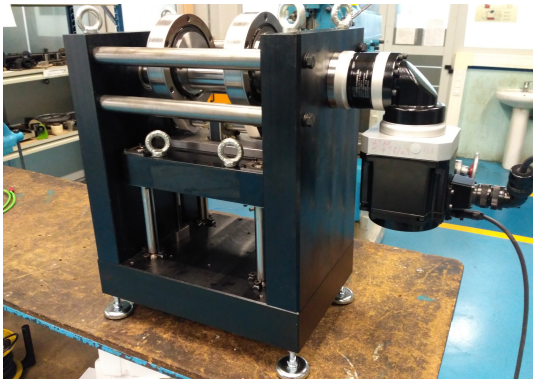

Fig. 5. The manufactured test bench.

Since the commercial assembly formed by the servomotor and the gearbox was selected to fulfill the maximum torque obtained in the optimization step, differences exit between the reduction ratio and the inertia of the different gears placed within the gearbox of the original servo press and the gearbox of the test bench. The industrial machine has three different reduction stages with the inertia values described by I_4, I_5 and I_6 shown in Table I. By contrast, the gearbox of the test bench has an inertia of $I_{gb} = 2.24{\times}10^{-4}kgm^2$. The reduction ratios of both gearboxes also differ, at $\eta = 49.13$ and $\eta = 7$ for the industrial machine and the test bench respectively. Nonetheless, despite these differences, the contribution of the gearbox to the dynamics of the servo press allows the kinematic and dynamic scaling of the test bench.

IV. EXPERIMENTAL RESULTS OF THE MANUFACTURED TEST BENCH

The dynamic and kinematic behavior of the test bench were compared with those of the original servo press. The dynamic behavior of the original servo press was monitored using two different force level strokes performed against two cylinders of rigid steel placed under each connecting rod, as shown in image A of Fig. 6. The two force levels were achieved by placing two rigid steel foils of different thicknesses on the rigid cylinders. The process force was measured using two piezoelectric sensors, each one installed in their respective connecting rod, and measuring the force signal at $1ksps$. The two maximum forces applied in both experiments were then $\lambda_{F_{ms}}$ proportionally replicated in the scaled test bench, using foils of different thicknesses placed on a rigid cylinder equipped with a load cell, as illustrated in image B of Fig. 6. Measurements were also carried out at $1ksps$.

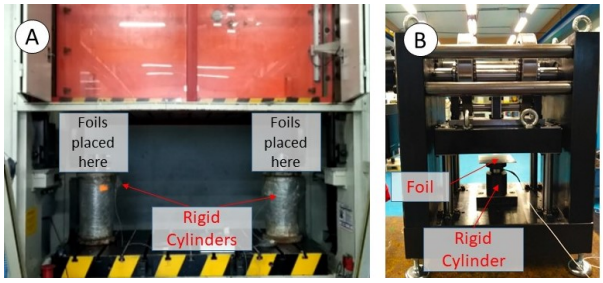

Fig. 6. Experimental set-up of the original servo press and the test bench.

Fig. 7 shows the two force profiles measured in the original servo press and the scaled test bench. The proportional force of the scaled test bench and the force of the original servo press in experiment A and experiment B, result in a similar force curve for the same angular position of the crankshaft, with a root-mean-square error (RMSE) value of $7.33t$ and $19.13t$, respectively. Comparing these RMSE values with the maximum force applied in both experiments, $182t$ in experiment A and $351t$ in experiment B, the obtained relative errors are 4.03% and 5.45% in experiment A and experiment B respectively, which yield an average value of 4.74% for the relative error. Therefore, the obtained relative error demonstrates the dynamic and kinematic similitude of the test bench with the original servo press.

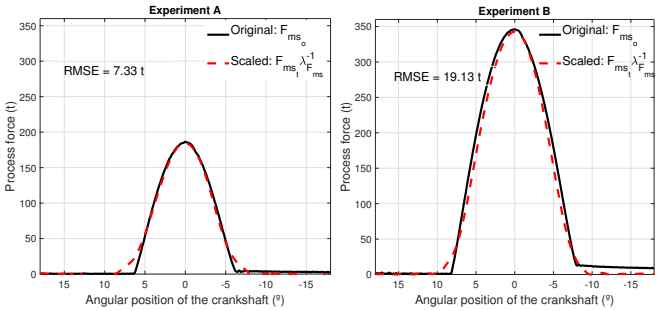

Fig. 7. Force profiles achieved in the original servo press and in the test bench, drawn throughout the angular position of the crankshaft.

Fig. 8 illustrates the curves for a force vs the linear position of the ram obtained in both experiments. The two curves in the test bench have a similar slope to those obtained in the industrial servo press. The differences noted at the beginning of the slope (around $2.5{\times}10^{-3}m$ and $1.5{\times}10^{-3}m$ in experiment A and around $3{\times}10^{-3}m$ and $2.5{\times}10^{-3}m$ in experiment B) are due to the differences in the dynamics of the load balancers of the test bench and industrial servo press.

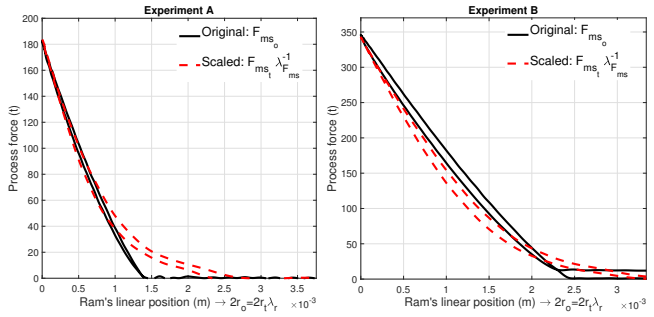

Fig. 8. Force profiles achieved in the original servo press and in the test bench, drawn throughout the linear displacement of the ram.

Fig. 9 shows the torque signals exerted by the servomotors of the industrial servo press and the test bench to generate the two force profiles illustrated in Fig. 7 in experiments A and B. The RMSE values for the portion of signal where the stroke is performed are, respectively, $1304.41Nm$ and $4346.9Nm$ in experiment A and B. Comparing the RMSE values with the peak to peak torque values of both experiments ($41323.58Nm$ in experiment A and $97643.53Nm$ in experiment B), the obtained relative errors are 3.16% and 4.45%, respectively.

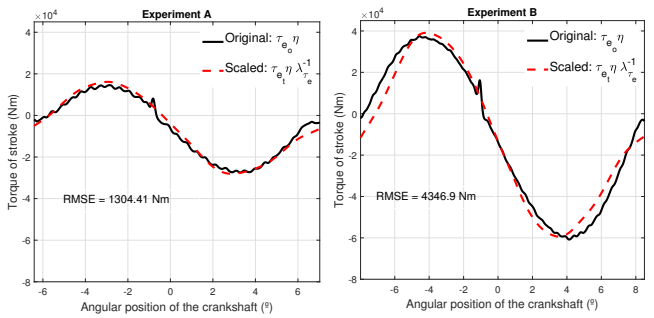

Fig. 9. Torque profiles achieved in the original servo press and in the test bench, drawn throughout the angular position of the crankshaft.

Fig. 10 illustrates the two speed profiles drawn by the crankshaft of the test bench and the original servo press in the two experiments shown in Fig. 7. As the reader may notice, slight deviations occur in the slopes of the speed profiles produced by the test bench and the industrial servo press. These differences are due to the different controllers and different non-proportional inertia of the kinematic chains that the servomotors have to move. The RMSEs of both experiments are also shown in the corresponding graphs for the two experiments; the RMSE are $3.12°/s$ and $3.44°/s$ for experiments A and B, respectively. Comparing these RMSE values with the maximum speed applied in both experiments, $60°/s$, the obtained relative errors are 5.2% and 5.73% in experiments A and B respectively.

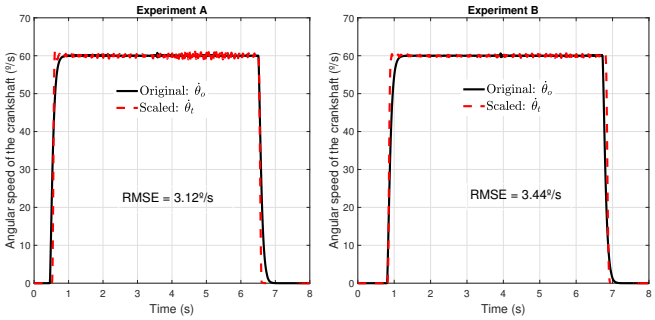

Fig. 10. Crankshaft speed profiles achieved in the original servo press and in the test bench, drawn throughout a complete working cycle.

V. Conclusion

The proposed design and manufacturing methodology provided a complete similitude-based scaling approach for building a scaled test bench that can emulate the dynamic and kinematic behavior of an original system. The proposed methodology goes beyond the conventional Buckingham's π scaling procedure, as it addresses integral design and manufacturing based on the optimization and activity analysis of physical magnitudes of the system. The optimization stage of the methodology eases the definition of the test bench's physical magnitudes, since the magnitude values are obtained according to the designer's requirements and constraints. The activity analysis sheds light on the relevance of each component in the dynamic behavior of the system, allowing a definition of the tolerances to ease the design and manufacturing of those components without creating significant alterations in the dynamic similitude.

The methodology was applied to construct a reduced scale test bench of an industrial servo press. The manufactured servo press test bench kept the dynamic similitude with the industrial servo press with a mean deviation of 4.74% in the emulated force profiles.

The methodology could also be improved to avoid possible distortion scenarios in the optimization step. Moreover, the scaling methodology proposed in this paper could be adopted for optimal scaling of other industrial machines while keeping the dynamic similitude with the original system. In addition, the parameter activity analysis may be useful in the design and manufacture of scaled test benches that can retain an efficient

and optimal energy consumption of their components for the required process. This may contribute to a savings in terms of the system's energy consumption.

APPENDIX A
CALCULATION OF A π-GROUP

This appendix addresses the calculation of a π-group formed by τ_e and the primary magnitudes F_{ms}, m_3 and r. The terms of (2) are replaced as in (17).

$$\begin{aligned} \pi_1 = \tau_e F_{ms}^{\alpha_1} m_3^{\alpha_2} r^{\alpha_3} \rightarrow \\ M^0 L^0 T^0 = M L^2 T^{-2} (M L T^{-2})^{\alpha_1} M^{\alpha_2} L^{\alpha_3} \end{aligned} \tag{17}$$

Developing the above expression, values of α_1, α_2 and α_3 are obtained so that a dimensionless π_1-group is formed as in (18).

$$\begin{aligned} M^0 L^0 T^0 = M^{1+\alpha_1+\alpha_2} L^{2+\alpha_1+\alpha_3} + T^{-2-2\alpha_1} \\ 0 = 1 + \alpha_1 + \alpha_2 \qquad \alpha_2 = 0 \\ 0 = 2 + \alpha_1 + \alpha_3 \qquad \alpha_3 = -1 \\ 0 = -2 - 2\alpha_1 \qquad \alpha_1 = -1 \\ \pi_1 = \tau_e F_{ms}^{-1} r^{-1} = \frac{\tau_e}{F_{ms} r} \end{aligned} \tag{18}$$

APPENDIX B
ANALYTIC EQUATIONS OF PARAMETERS' POWER

This section of gathers the analytical expression of the power of servo press's parameters defined as in 19.

$$P_x = \frac{d}{dt} E_x \qquad x = 1, 2, ...X \tag{19}$$

The analytical expressions of the parameter power are defined on the basis of the angular position of the crankshaft $\theta(t)$. Analytical expressions of the power of the servo press parameters are shown in the set of equations (20-25), where $\theta(t), \dot{\theta}(t)$ and $\ddot{\theta}(t)$ are defined as $\theta, \dot{\theta}$ and $\ddot{\theta}$ respectively for the sake of simplicity.

$$P_{I_1} = I_1 \ddot{\theta} \dot{\theta} \tag{20}$$

$$P_{I_2} = I_2 \ddot{\theta} \dot{\theta} c^2 \tag{21}$$

$$P_{\xi} = \xi x \dot{x} \tag{22}$$

$$P_{m_1} = g m_1 \acute{r} \dot{\theta} \sin\theta \tag{23}$$

$$\begin{aligned} P_{m_2} = & \frac{m_2 (l - \acute{l})^2 r^2 \ddot{\theta} \dot{\theta} \cos^2\theta}{l^2} - \frac{m_2 \left(l - \acute{l}\right)^2 r^2 \dot{\theta}^3 \cos\theta \sin\theta}{l^2} \\ & + m_2 \left(-r\theta \sin\theta - \frac{\acute{l} r^2 \theta \cos\theta \sin\theta}{lc} \right) \left(-r\ddot{\theta} \sin\theta \right. \\ & -r\dot{\theta}^2 \cos\theta - \frac{\acute{l} r^2 \ddot{\theta} \cos\theta \sin\theta}{lc} + \frac{\acute{l} r^2 \dot{\theta}^2 \sin^2\theta}{lc} \\ & \left. -\frac{\acute{l} r^4 \dot{\theta}^2 \cos^2\theta \sin^2\theta}{lc^3} - \frac{\acute{l} r^2 \dot{\theta}^2 \cos^2\theta}{lc} \right) \\ & - g m_2 \left(-r\dot{\theta} \sin\theta - \frac{\acute{l} r^2 \dot{\theta} \cos\theta \sin\theta}{lc} \right) \end{aligned} \tag{24}$$

$$\begin{aligned} P_{m_3} = & m_3 \left(-r\dot{\theta} \sin\theta - \frac{r^2 \dot{\theta} \cos\theta \sin\theta}{c} \right) \left(-r\ddot{\theta} \sin\theta \right. \\ & -r\dot{\theta}^2 \cos\theta - \frac{r^2 \ddot{\theta} \cos\theta \sin\theta}{c} + \frac{r^2 \dot{\theta}^2 \sin^2\theta}{c} \\ & \left. -\frac{r^4 \dot{\theta}^2 \cos^2\theta \sin^2\theta}{c^3} - \frac{r^2 \dot{\theta}^2 \cos\theta^2}{c} \right) - g m_3 \\ & \left(-r\dot{\theta} \sin\theta - \frac{r^2 \dot{\theta}^2 \sin\theta \cos\theta^2}{c} \right) \end{aligned} \tag{25}$$

REFERENCES

[1] B. Kittirungsi, *A scaling methodology for dynamic systems: Quantification of approximate similitude and use in multiobjective design*. ProQuest, 2008.

[2] W. Zhang, J. Wang, and Y. Lin, "Integrated design and operation management for enterprise systems," *Enterprise Information Systems*, vol. 13, no. 4, pp. 424–429, 2019. DOI: 10.1080/17517575.2019.1597169.

[3] S. Brennan and A. Alleyne, "Using a scale testbed: Controller design and evaluation," *IEEE Control Systems Magazine*, vol. 21, no. 3, pp. 15–26, 2001.

[4] E. Esteban, O. Salgado, A. Iturrospe, and I. Isasa, "Design methodology of a reduced-scale test bench for fault detection and diagnosis," *Mechatronics*, vol. 47, pp. 14–23, 2017.

[5] C. P. Coutinho, A. J. Baptista, and J. D. Rodrigues, "Reduced scale models based on similitude theory: A review up to 2015," *Engineering Structures*, vol. 119, pp. 81–94, 2016.

[6] R. Doraiswami and L. Cheded, "Robust model-based soft sensor: Design and application," *IFAC Proceedings Volumes*, vol. 47, no. 3, pp. 5491–5496, 2014. DOI: 10.3182/20140824-6-ZA-1003.00245.

[7] E. Esteban, O. Salgado, A. Iturrospe, and I. Isasa, "Model-based approach for elevator performance estimation," *Mechanical Systems and Signal Processing*, vol. 68, pp. 125–137, 2016.

[8] A. Vaschy, "Sur les lois de similitude en physique," in *Annales télégraphiques*, vol. 19, 1892, pp. 25–28.

[9] G. J. Simitses and J. Rezaeepazhand, "Structural similitude and scaling laws for laminated beam-plates," 1992.

[10] R. Verma, D. Del Vecchio, and H. K. Fathy, "Development of a scaled vehicle with longitudinal dynamics of an hmmwv for an its testbed," *IEEE/ASME Transactions on Mechatronics*, vol. 13, no. 1, pp. 46–57, 2008.

[11] P. Novak, V. Guinot, A. Jeffrey, and D. E. Reeve, *Hydraulic modelling: An introduction: Principles, methods and applications*. CRC Press, 2018.

[12] Z. Luo, Y. Wang, J. Zhai, Y. Zhu, and D. Wang, "Prediction of vibration characteristics of blisks using similitude models," *Mechanics Based Design of Structures and Machines*, vol. 47, no. 2, pp. 121–135, 2019.

[13] Z. Luo, Y. Zhu, X. Zhao, and D. Wang, "Determination method of dynamic distorted scaling laws and applicable structure size intervals of a rotating thin-wall short cylindrical shell," *Proceedings of the Institution of Mechanical Engineers*, vol. 229, no. 5, 2015.

[14] Z. Luo, Y. Zhu, X. Zhao, and D. Wang, "Determining dynamic scaling laws of geometrically distorted scaled models of a cantilever plate," *Journal of Engineering Mechanics*, vol. 142, no. 4, 2016.

[15] F. He, Z. Luo, L. Li, and Y. Zhang, "A similitude for the middle-frequency vibration response of satellite solar array based on the wave coupling hybrid finite element–statistical energy analysis method," *Proceedings of the Institution of Mechanical Engineers*, vol. 203-210, 2020. DOI: 10.1177/0954406220916491.

[16] L. L. Zhou and D. K. Li, "Design of scaled model for dynamic characteristics of stiffened cylindrical shells based on equivalent similar method," *The Aeronautical Journal*, vol. 123, no. 1261, pp. 398–415, 2019. DOI: 10.1017/aer.2018.154.

[17] Q. Li, W. Zhang, and L. Chen, "Design for control-a concurrent engineering approach for mechatronic systems design," *IEEE/ASME transactions on mechatronics*, vol. 6, no. 2, pp. 161–169, 2001.

[18] E. Buckingham, "On physically similar systems; illustrations of the use of dimensional equations," *Physical review*, vol. 4, no. 4, p. 345, 1914.

[19] W. Curtis, J. D. Logan, and W. Parker, "Dimensional analysis and the pi theorem," *Linear Algebra and its Applications*, vol. 47, pp. 117–126, 1982.

[20] H.-C. Wu, "The karush–kuhn–tucker optimality conditions in an optimization problem with interval-valued objective function," *European Journal of Operational Research*, vol. 176, no. 1, pp. 46–59, 2007, ISSN: 0377-2217. DOI: https://doi.org/10.1016/j.ejor.2005.09.007.

[21] J. Olaizola, C. Bouganis, E. Saenz de Argandoña, A. Iturrospe, and J. M. Abete, "Real-time servo press force estimation based on dual Particle Filters," *IEEE Transactions on Industrial Electronics*, pp. 1–1, 2019. DOI: 10.1109/TIE.2019.2921292.

Jon Olaizola was born in Azkoitia (Gipuzkoa) Spain in 1992. He received the Master's Degree in Embedded Systems of Mondragon Unibertsitatea, Spain in 2016. He obtained the PhD in metal forming facility monitoring based on soft sensors in 2020, which has motivated the preset paper.

He is currently within the Signal Theory and Communications research group at Mondragon Unibertsitatea of Arrasate. His research field includes modelling, signal processing and hardware implementation.

Ekaitz Esteban obtained the title in Industrial Engineering by the University of Mondragon, where he later defended his doctoral thesis. His doctoral thesis was focused on the monitoring of elevators using virtual sensors whose purpose was to develop strategies of predictive maintenance in elevators. Currently, he works as researcher academic staff within the group of Acoustics and Vibrations of the University of Mondragon.

Javier Trinidad was born in Elorrio (Bizkaia) Spain in 1983. He got his PhD degree in 2013 in Mondragon University. His research in the university and in the industry has been focused in characterization techniques, manufacturing processes and mechanical design. He currently works at the Mechanics and Industrial Manufacturing Department. Within this department he combines teaching activities with research activities within the Advanced Processes for Material Forming research group.

Aitzol Iturrospe received his an Engineer in Automatics and Electronics (MSc) and PhD degrees from the University of Mondragon.

After finishing his PhD studies, which focused on signal processing applied to industrial processes and systems monitoring, he was a visiting researcher at the Laboratory for Manufacturing and Sustainability (LMAS) at the University of California in Berkeley. He is currently a member of the Signal Theory and Communications area at the University of Mondragon. His research focuses on signal processing applied to Non-Destructive Testing (NDT) and health monitoring applications (as well as on the development of sensors and measurement systems).

Lander Galdos was born in Mondragon, Spain in 1978. He received the Ph.D. degree in Manufacturing Processes from Mondragon Unibertsitatea in 2007.

From 2007 he is lecturer and researcher at Mondragon Unibertsitatea within the Advanced Material Forming Processes research group. He is currently the coordinator of this research group. His research field includes the material, tribological and processes modelization in the field of metal forming processes.

Jose Manuel Abete was born in Tolosa, Spain, in 1962. He received the title of Industrial Engineer from the University of Navarra, San Sebastián, Spain, in 1986 and the Ph.D. in Industrial Engineering from the University of Navarra, San Sebastián, Spain, in 1994.

He worked as a researcher in Applied Mechanics at Ceit, San Sebastián, Spain, from 1990 to 1995. In 1995 he joined the MGEP of Mondragon University, where he is currently professor of Mechanical Vibrations. His research interests include modelling, analysis and control of mechatronic systems.

Eneko Sáenz de Argandoña was born in Vitoria-Gasteiz, Spain in 1978. He received the Ph.D. degree in Manufacturing Processes from Mondragon Unibertsitatea in 2009. From 2009 he is lecturer and researcher at Mondragon Unibertsitatea within the Advanced Material Forming Processes research group.

His research field includes the material, tribological and processes modelization in the field of metal forming processes.